Ductility and Energy Dissipation Capacity of Shear-Dominated Steel Plate Walls

In-Rak Choi[1] and Hong-Gun Park[2]

Abstract: An experimental study was performed to investigate the potential maximum ductility and energy dissipation capacity of steel plate walls with thin infill plates. Three specimens of a three-story steel plate wall were tested. A concentrically braced frame (CBF) and a moment-resisting frame (MRF) were also tested for comparison. To maximize the ductility and energy dissipation capacity of the steel plate walls, ductile details were used. The test parameters were the aspect ratio of the infill plate and the shear strength of the column. The steel plate walls exhibited much better ductility and energy dissipation capacity as compared to the CBF and MRF. This result indicates that unlike conventional reinforced concrete walls and CBFs, shear-dominated steel plate walls with thin infill plates possess excellent ductility capacity as well as high strength and stiffness. Based on the results of previous studies and the present study, the variations in the ductility and the energy dissipation capacity of the steel plate walls according to the design parameters were investigated.

DOI: 10.1061/(ASCE)0733-9445(2008)134:9(1495)

CE Database subject headings: Steel plates; Shear walls; Cyclic tests; Ductility; Energy; Parameters.

Introduction

The framed steel plate wall that consists of frame members and infill plates is a structurally effective and economical lateral load resisting system. The framed steel plate wall has advantages over the conventional reinforced concrete wall in several aspects. The overall weight of a structure can be significantly reduced by using the steel plate wall. Therefore, the size of the foundation and the earthquake load can be reduced. Further, structures can be constructed faster with the use of the steel plate wall. Also, the usable floor area can be increased by using the steel plate wall with thin infill plates.

Research on the framed steel plate wall started in the early 1970s in the United States, Canada, and Japan. In Japan, generally, the infill plate has been designed as either a stiffened plate or a thick plate to prevent the local buckling of the infill plate and to support a gravity load (Astaneh-Asl 2001). However, the use of plate stiffeners and thick plates is not economical because of the high cost involved in their fabrication and construction. For this reason, in the United States and Canada, feasibility of the steel plate wall with unstiffened thin infill plates has been studied. Because of the thin infill plates, the postbuckling diagonal tension-field action of the infill plates was utilized in the walls.

Generally, in a cantilever wall (flexure-dominated wall) with stiffened plates or thick plates, the major part of its inelastic deformation develops at the wall base [Fig. 1(a)]. On the other hand, the framed steel plate wall with unstiffened thin infill plates can be designed as a shear-dominated wall so that the thin infill plates in multiple stories yield by the shear action before the boundary columns at the wall base yield by the cantilever action. Therefore, like the moment-resisting frame (MRF), yielding by the shear action can be distributed along the wall height [Fig. 1(b)]. As a result, the shear-dominated wall exhibits excellent ductility as well as high strength. The shear-dominated steel plate wall can be considered as an ideal earthquake-resisting system that has both high strength and ductility.

The framed steel plate walls without plate stiffeners have been studied by many researchers (Caccese et al. 1993; Driver et al. 1997; Elgaaly 1998; Lubell et al. 2000; Behbahanifard 2003; Park et al. 2007). The principal parameters in previous tests were the span-to-thickness ratio of the infill plate, type of the beam-to-column connection (moment or shear connection), and the connection details between the infill plate and the frame members (welded or bolted connection). Table 1 summarizes the previous tests for multiple-story framed steel plate walls. The behavioral characteristics of the steel plate walls have been studied on the basis of these tests.

However, several aspects of the structural performance of the steel plate wall with thin infill plates need to be clarified. As presented in Table 1, the plate aspect ratios (span-to-story height ratio of an infill plate, l_p/h_p) of the previous test specimens were relatively small, ranging from 1.0 to 1.8. Further, the sizes of the frame members used in the previous tests were relatively large so that the moment frame action significantly contributed to the overall behavior of the steel plate wall specimens. In Driver et al. (1997), span length $l=3.05$ m, column depth $d_c=314$ mm, and $l/d_c=9.7$; in Park et al. (2007), $l=1.5$ m, $d_c=250$ mm, and $l/d_c=6.0$. However, in many buildings, the span-to-story height ratio is greater than 2.0, and the ratio of the span to column depth (l/d_c) ranges from 20 to 30. Therefore, the steel plate walls having their plate aspect and span-to-column depth ratios within such practical ranges need to be tested (AISC 2005).

Table 1 presents the roof displacement ductility and the maxi-

[1]Graduate Student, Dept. of Architecture, Seoul National Univ., San 56-1, Shinlim-Dong, Kwanak-Gu, Seoul 151-744, South Korea.

[2]Associate Professor, Dept. of Architecture, Seoul National Univ., San 56-1, Shinlim-Dong, Kwanak-Gu, Seoul 151-744, South Korea. E-mail: parkhg@snu.ac.kr

Note. Associate Editor: Benjamin W. Schafer. Discussion open until February 1, 2009. Separate discussions must be submitted for individual papers. The manuscript for this paper was submitted for review and possible publication on March 5, 2007; approved on January 28, 2008. This paper is part of the ***Journal of Structural Engineering***, Vol. 134, No. 9, September 1, 2008. ©ASCE, ISSN 0733-9445/2008/9-1495–1507/$25.00.

J. Struct. Eng. 2008.134:1495-1507.

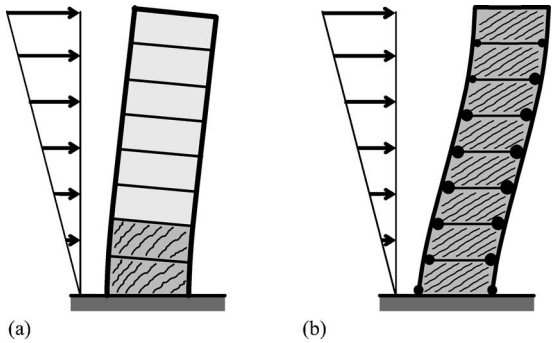

Fig. 1. Deformation characteristics of steel plate walls: (a) flexure-dominated wall; (b) shear-dominated wall

mum interstory drift ratio of the steel plate wall specimens tested in the previous studies. The roof displacement ductility is defined as the ratio of the maximum roof displacement to the yield roof displacement of the specimens. In Table 1, the roof displacement ductility ranges from 1.5 to 12.4, and the maximum interstory drift ratio ranges from 1.0 to 5.4. The wide range of the roof displacement ductility and the maximum interstory drift ratio indicates that the behavior of the steel plate walls significantly varies according to their design parameters and details. According to Caccese et al. (1993) and Park et al. (2007), the ductility of steel plate walls with thin infill plates is determined by the strength and compactness of their boundary columns that resist the tension-field action of the infill plates. Elgaaly (1998) and Park et al. (2007) reported that in order to maximize the ductility capacity of a steel plate wall, the yielding of the infill plates by shear action must precede the yielding of the boundary columns by increasing the overall flexural capacity of the wall. The results of the previous studies indicate that in order to accurately evaluate the earthquake resistance of the steel plate walls and the resulting performance-based earthquake load, the trend of the wall ductility according to the design parameters must be clarified. Further, the potential maximum ductility of the steel plate walls that can be attained by using ductile details needs to be investigated.

In the present study, three-story steel plate walls were tested to study the potential maximum ductility and energy dissipation capacity of the shear-dominated steel plate wall. As the test specimens are reduced small-scale models of the prototype walls and the welds used in the specimens are of higher quality than those used in the field condition, it is difficult to quantitatively evaluate the structural performance of the full-scale steel plate walls from the test results. Therefore, in the present study, for comparison with the test results of the reduced-scale steel plate walls, a concentrically braced frame (CBF) and an MRF were tested. Based on previous test results and the results of the present study, the variations of the wall ductility and energy dissipation capacity according to the design parameters were studied.

Specimens and Test Setup

The test specimens were one-third models of a three-story prototype wall with thin infill plates. The configuration of the test specimens is presented in Table 2 and Fig. 2. To investigate the potential maximum ductility of the steel plate walls, the steel plate wall specimens were designed with the ductile details proposed in previous studies and the present study—seismic compact column sections, full-penetration weld connection at the beam-to-column joints, column strength and column stiffness for resisting the tension-field action of the infill plates, and ductile details in the weld connection between plates and frame members (ductile

Table 1. Previous Tests for Multiple-Story Steel Plate Wall

Researcher	Specimen	Number of stories	Loading point	Gravity load (kN)	Plate thickness (mm)	Aspect ratio of plate[a]	Column section	Infill plate connection	Displ. ductility[b]	Maximum interstory drift (%)
Caccese et al. (1993)	M22	3	Top	—	0.76	1.5	W100×19	Weld	12.4	5.4[c]
	M14	3	Top	—	1.87	1.5	W100×19	Weld	4.0	2.0[c]
	M12	3	Top	—	2.65	1.5	W100×19	Weld	2.7	1.7[c]
	S22	3	Top	—	0.76	1.5	W100×19	Weld	4.4	3.9[c]
	S14	3	Top	—	1.95	1.5	W100×19	Weld	2.6	1.8[c]
Driver et al. (1997)	—	4	Each floor	1,440	4.8	1.7	W310×118	Weld	4.7	4.0
Elgaaly (1998)	SWT11	2	Top	445	2.28	1.2	W150×22	Bolt	3.6	2.1[c]
	SWT12	2	Top	—	2.28	1.2	W150×22	Bolt	3.5	2.1[c]
	SWT13	2	Top	445	2.28	1.2	W150×22	Bolt	3.4	1.8[c]
	SWT14	2	Top	445	2.28	1.2	W150×22	Weld	3.6	1.8[c]
	SWT15	2	Top	445	2.28	1.2	*W*150×30	Bolt	4.3	2.4[c]
Lubell et al. (2000)	SPSW4	4	Each floor	54	1.5	1.0	S75×8	Weld	1.5	1.0
Behbahanifard (2003)	—	3	Each floor	1,080	4.8	1.8	W310×118	Weld	4.5	3.4
Park et al. (2007)	SC2T	3	Top	—	2	1.5	H-250×250×20×20[d]	Weld	6.4	3.8
	SC4T	3	Top	—	4	1.5	H-250×250×20×20[d]	Weld	4.4	2.7
	SC6T	3	Top	—	6	1.5	H-250×250×20×20[d]	Weld	3.8	2.8
	WC4T	3	Top	—	4	1.5	H-250×250×9×12[d]	Weld	3.8	2.3
	WC6T	3	Top	—	6	1.5	H-250×250×9×12[d]	Weld	2.7	1.4

[a]Span-to-height ratio of an infill plate (l_p/h_p).

[b]Maximum roof displacement divided by yield roof displacement ($=\delta_{max}/\delta_y$).

[c]Average story drift ($=\delta_{max}/h$).

[d]Wide flange section, H-depth × width × web thickness × flange thickness.

J. Struct. Eng. 2008.134:1495-1507.

Table 2. Test Specimens

Specimen	Plate thickness (steel grade)	Aspect ratio of plate	Column section (steel grade)
FSPW1	4 mm (SS400[a])	1.5	H-150×150×22×22[b] (SM490[c])
FSPW2	4 mm (SS400[a])	2.2	H-150×150×22×22[b] (SM490[c])
FSPW3	4 mm (SS400[a])	2.2	H-150×150×8× 20[b] (SM490[c])
CBF[e]	H-100×100×10×10[d] (SS400[a])	—	H-150×150×22×22[b] (SM490[c])
MRF[f]	—	—	H-150×150×22×22[b] (SM490[c])

[a]SS400 (Korean standard):F_y=240 MPa, F_u=400–510 MPa.

[b]Wide flange section, H-depth × width × web thickness × flange thickness.

[c]SM490 (Korean standard):F_y=330 MPa, F_u=490–610 MPa.

[d]Brace section.

[e]Concentrically braced frame.

[f]Moment-resisting frame.

fish-plate detail). The test parameters were the aspect ratio of the infill plates and the shear capacity of the columns.

The thickness of the infill plates in all the wall specimens was 4 mm (Korean Standard SS400, F_y=240 MPa). To investigate the effect of the aspect ratio of the infill plates, the control specimen FSPW2 [Fig. 2(b)] was designed to have a typical aspect ratio (l_p/h_p)=2.2 (l_p=2,200 mm, h_p=1,000 mm) of the prototype wall. For comparison, the aspect ratio of specimen FSPW1 [Fig. 2(a)] was 1.5, which was the same as that used in the specimens of Caccese et al. (1993) and Park et al. (2007).

The frame members were built-up sections made of SM490 steel (Korean Standard, F_y=330 MPa). All columns, except those used in specimen FSPW3, were H-150×150×22×22 mm [built-up wide flange section, H-overall depth (d_c)×flange width (b_f)×web thickness (t_w)×flange thickness (t_f)]. The beams at the second and third stories were H-150×100×12×20. The top beam that was connected to the actuator was H-250×150×12×20. The flange and web elements of all beams and columns satisfied the requirements for the seismic compact section according to the AISC Seismic Provisions (AISC 2005). In particular, the column flange was designed with a very small width-thickness ratio ($b_f/2t_f$=3.4 for FSPW1 and FSPW2 and 3.8 for FSPW3) for the following two reasons: (1) to study the potential maximum ductility of the steel plate walls, the local buckling of the columns was prevented even after the yielding of the column flanges; and (2) to reduce the contribution of the moment-resisting frame action to the overall behavior of the steel plate wall, the depth and width of the column section were reduced, whereas the cross-sectional area required for the flexural strength of the wall was maintained.

The columns in FSPW1 and FSPW2 were designed to have sufficient flexural and shear strengths for resisting the tension-field action of the infill plate. According to Park et al. (2007), the bending moment and shear force applied to the top and bottom ends of a column by the tension-field action of the infill plate can be approximately calculated as $M_u=(f_{py}th_s^2\sin^2\alpha)/12$ and $V_u=0.25f_{py}th_s\sin^2 2\alpha$, where f_{py}=yield strength of the infill plate; t=thickness of the infill plate; h_s=story height; and α=inclination angle of the tension-field [Eq. (10)].

FSPW3 was tested to investigate the effect of the shear capacity of the columns on the ductility of the steel plate walls. In FSPW3, the shear capacity of its columns (H-150×150×12×20) was 60% of the shear strength required to resist the tension-field action of the infill plate. However, the columns satisfied the requirements of the seismic compactness of the flange and web elements and the stiffness of the vertical boundary elements for the steel plate walls, as specified by the AISC Seismic Provisions (AISC 2005).

For the ductile behavior of the beam-to-column joints, fully restrained moment connections were used. The beam flange was rigidly connected to the column by full penetration groove welding. The beam web was connected to the column flange by two-side fillet welding. The infill plates were weld connected to the boundary frame members using 50-mm-wide and 6-mm-thick fish plates. The fish plates were welded to the beams and columns by two-side fillet welding (Fig. 2). In the present study, to enhance the ductility capacity of the steel plate wall, the fish plate was improved. Fig. 3 compares the weld-connection details of the fish plates that were used in the previous study [Park et al. (2007)] and in the present study. In the specimens tested in the present study, the welded joint of the fish plates was moved from the corner of the infill plate toward the midspan of the wall in order to prevent early fracture due to stress concentration at the joints [Fig. 3(b)].

The CBF and MRF consisted of beams and columns with the same sizes as those used for FSPW2. For comparison with the test results of the steel plate walls, the braces (H-100×100×10×10) in the CBF were designed to have the same steel weight as that used for the infill plate of FSPW2. The slenderness ratio of the brace was KL/r=27, which is classified as a stocky brace. The brace members satisfied the requirements for the slenderness and seismic compactness of special CBFs, as specified by the AISC Seismic Provisions (AISC 2005).

The average results of the coupon tests for the materials used in this test are presented in Table 3. Three coupons were tested for each material. Before testing the steel plate walls, a pushover analysis was performed for the specimens by using ABAQUS (HKS 2003). From the results, the yield displacement δ_y at the top of the specimens was estimated to be 15 mm on average. Based on the predicted yield displacement δ_y (15 mm), the target displacements for the cyclic loading were chosen as $\pm 0.2\delta_y$, $0.4\delta_y$, $0.6\delta_y$, $0.8\delta_y$, $1.0\delta_y$, $1.5\delta_y$, $2\delta_y$, $3\delta_y$, $4\delta_y$, $6\delta_y$, $8\delta_y$, $10\delta_y$, and $12\delta_y$. Cyclic loadings were repeated three times at each target displacement.

Test Results

Load–Displacement Relationship

Fig. 4 shows the load–top displacement relationships of the test specimens and the results predicted by ABAQUS. Fig. 4(f) shows a comparison of the envelope curves of the load–top displacement

J. Struct. Eng. 2008.134:1495-1507.

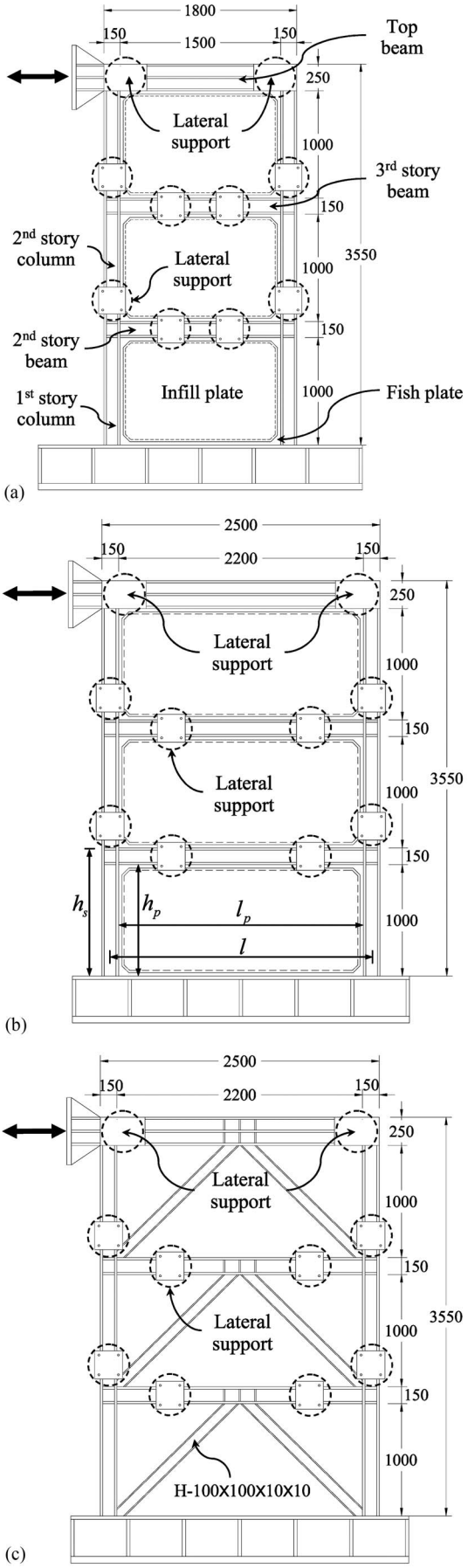

Fig. 2. Dimensions of specimens (mm): (a) FSPW1; (b) FSPW2; and (c) CBF (concentrically braced frame)

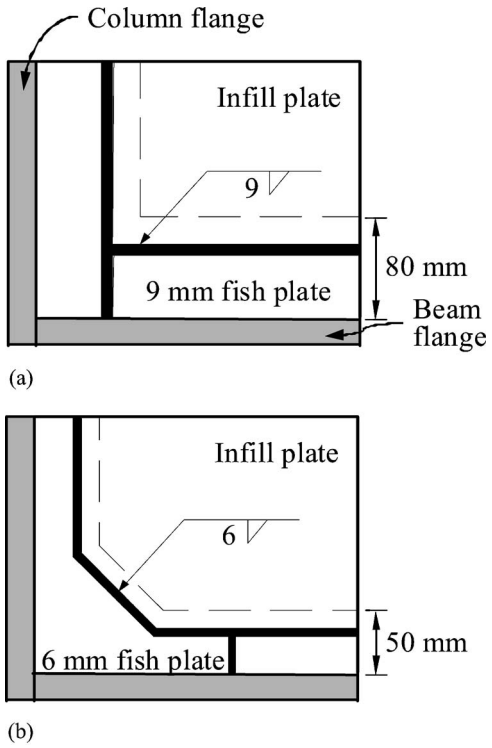

Fig. 3. Weld connection details of fish plate: (a) adapted from Park et al. (2007); (b) present study

relationships of the specimens. The test results at the yield point, maximum load, and maximum displacement of the specimens are presented in Table 4. The yield point (δ_y, P_y) was defined using the concept of equal plastic energy so that the area enclosed by the idealized elastoplastic envelope curve was the same as that enclosed by the actual envelope curve [Fig. 4(f)]. The maximum displacement (δ_{max}) of the CBF specimen showing a softening behavior was defined as the postpeak displacement corresponding to 0.8 times the maximum load.

As shown in Fig. 4, the steel plate wall specimens showed a large initial stiffness and load-carrying capacity. FSPW2, which had a relatively large aspect ratio (l_p/h_p=2.2), sufficient column strength for resisting the tension-field action, and seismic compact column sections, exhibited the greatest load-carrying capacity and deformation capacity [Fig. 4(b)]. On the other hand, FSPW1 with relatively small plate aspect ratio (l_p/h_p=1.5) showed less load-carrying capacity than FSPW2 [Fig. 4(a)] did. FSPW3 with insuf-

Table 3. Results of Tensile Coupon Test

Grade	Thickness (mm) Nominal	Thickness (mm) Actual	Yield stress (MPa)	Ultimate stress (MPa)	Yield strength ratio[a] (%)	Member
SS400	4	3.9	299	372	80	Infill panel
SS400	10	9.6	393	571	76	Brace
SM490	6	6.1	407	556	73	Fish plate
SM490	8	8.1	385	542	71	Column
SM490	12	12.1	377	527	72	Beam
SM490	20	20.1	353	538	66	Beam, column
SM490	22	21.7	348	522	67	Column

[a]Yield stress/ultimate stress.

J. Struct. Eng. 2008.134:1495-1507.

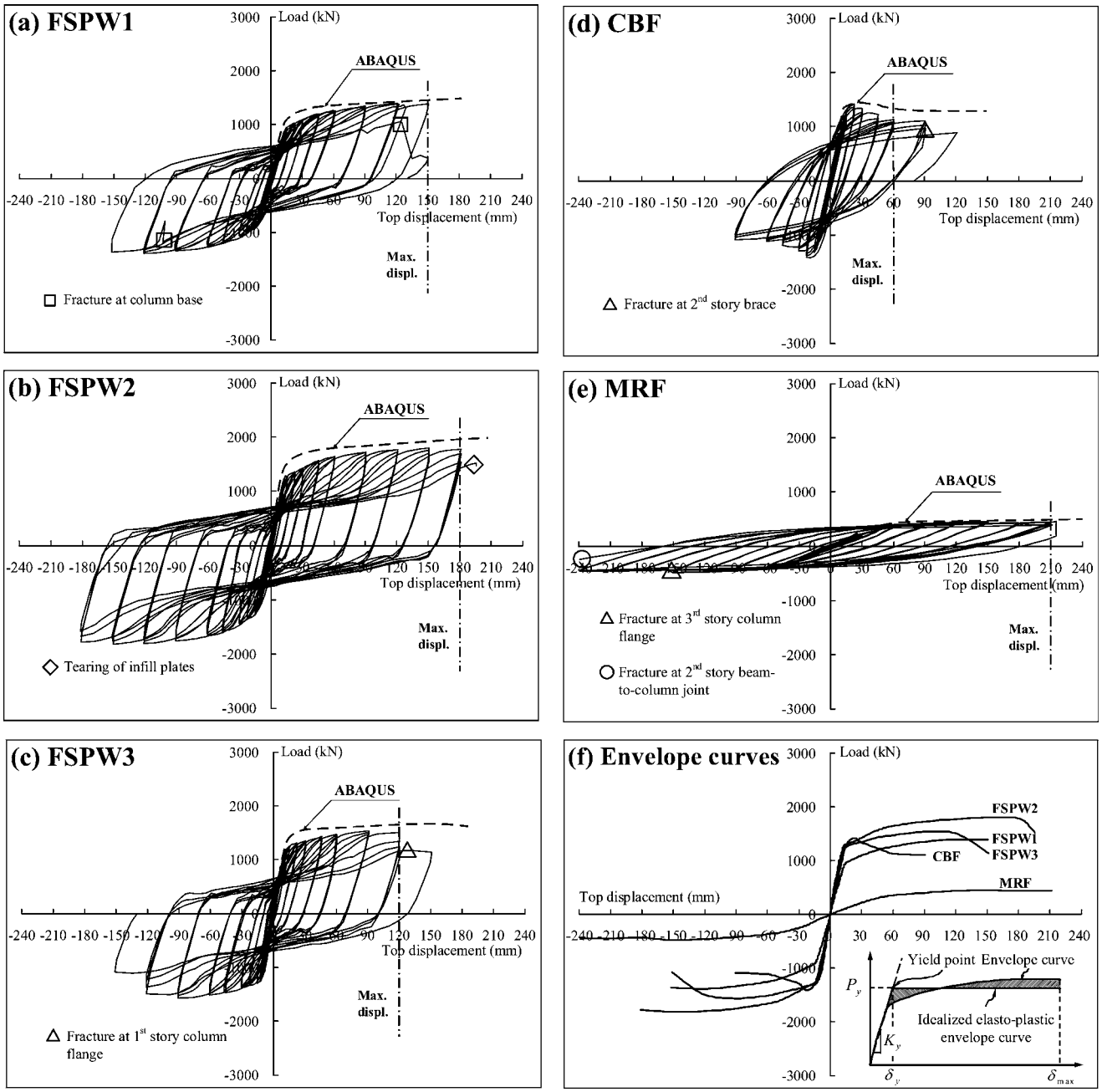

Fig. 4. Load–top displacement relationships of test specimens

ficient column shear strength showed the least deformation capacity among the steel plate wall specimens [Fig. 4(c)].

Fig. 5 shows the results of the SC specimens—SC2T and SC4T—tested in a previous study by Park et al. (2007). The results in Figs. 4 and 5 indicate that the FSPW specimens with smaller column sections and lower infill plate strength exhibited less load-carrying capacity and more pinched behavior than the SC specimens did. On the other hand, the FSPW specimens showed better deformation capacity. As indicated by Caccese et al. (1993) and Park et al. (2007), the superior deformation capacity of the FSPW specimens is mainly due to (1) low width-thickness ratio of the column flange ($b_f/2t_f$) that prevented local buckling and (2) the use of thin infill plates that reduced the flexural demand of the wall.

Figs. 4(d and e) show the test results of the CBF and MRF. The CBF showed considerably low deformation capacity because of the early buckling of the compression braces. The MRF exhibited large deformation capacity. However, more important, as its initial stiffness and strength were relatively low, the ductility of the MRF (δ_{max}/δ_y=3.58 in Table 4) was significantly less than that of FSPW2 (δ_{max}/δ_y=11.70).

Failure Mechanism

The failure mechanisms of the specimens are briefly described in Fig. 4. The deformed shapes of the specimens are shown in Figs. 6–8. In FSPW1 and FSPW2, during early loading, tension-field action developed due to the local buckling of the infill plate. Subsequently, the yielding of the infill plates by the shear action propagated along the wall height [Fig. 6(a)]. After the yielding of all the infill plates, plastic hinges were developed at the beam ends and the first-story column base by the moment frame action.

J. Struct. Eng. 2008.134:1495-1507.

Table 4. Test Results

	Maximum load						Maximum displacement					
	Positive loading (+)			Negative loading (–)			Positive loading (+)			Negative loading (–)		
Specimen	P_{max} (kN)	δ (mm)	Story drift[a] (%)	P_{max} (kN)	δ (mm)	Story drift[a] (%)	P (kN)	δ_{max} (mm)	Story drift[a] (%)	P (kN)	δ_{max} (mm)	Story drift[a] (%)
FSPW1	1,392	121.5	3.6	−1,388	−121.3	3.6	1,383	150.9	4.5	−1,364	−152.1	4.5
FSPW2	1,798	150.9	4.5	−1,817	−150.8	4.5	1,776	181.3	5.4	−1,776	−181.5	5.4
FSPW3	1,531	91.3	2.7	−1,565	−90.8	2.7	1,500	120.6	3.6	−1,490	−121.1	3.6
CBF	1,419	22.8	0.7	−1,421	−19.2	0.6	1,125	60.7	1.8	−1,115	−60.8	1.8
MRF	453	150.7	4.5	−483	−149.1	4.4	391	211.4	6.3	−450	−241.5	7.2

	Yield point								P_{max}/P_y		δ_{max}/δ_y (Displ. ductility)	
	Positive loading (+)				Negative loading (–)							
Specimen	P_y (kN)	δ_y (mm)	Story drift[a] (%)	K_y[b] (kN/mm)	P_y (kN)	δ_y (mm)	Story drift[a] (%)	K_y[b] (kN/mm)	Positive loading	Negative loading	Positive loading	Negative loading
FSPW1	1,252	18.0	0.53	70	−1,257	−18.8	0.56	67	1.11	1.10	8.38	8.09
FSPW2	1,653	15.5	0.46	107	−1,651	−15.4	0.46	107	1.09	1.10	11.70	11.78
FSPW3	1,458	14.1	0.42	103	−1,470	−13.3	0.39	111	1.05	1.06	8.55	9.11
CBF	1,272	14.3	0.42	89	−1,256	−13.5	0.40	93	1.12	1.13	4.24	4.50
MRF	419	59.0	1.75	7	−430	−47.5	1.41	9	1.08	1.12	3.58	5.08

[a]Maximum displacement at top divided by wall height.

[b]Elastic stiffness $K_y = P_y/\delta_y$.

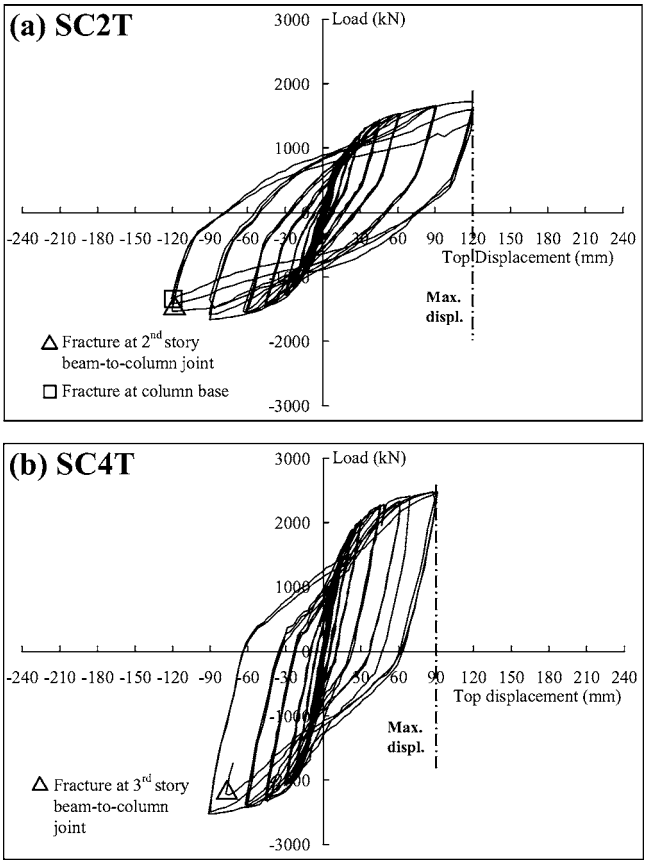

Fig. 5. Load–top displacement relationships of SC specimens (Park et al. 2007)

In FSPW1, at 4.5% drift (top displacement=150 mm), a fracture occurred at the welded connection of the column base. The fracture was initiated in the heat-affected weld zone of the outer column flange that was connected to the base plate, and it propagated to the column web and the fish plate. According to Driver et al. (1998), the fracture of the column flanges at the wall base is developed by the combined actions of local buckling, subsequent cyclic bending, and triaxial tensile stress concentration (Blodgett 1995). However, in actual buildings, generally, columns at the first story are directly connected to the basement columns rather than being fixed to the column base. Therefore, such a sudden fracture at the column base is unlikely to occur.

FSPW2 exhibited excellent ductility without any sudden decrease in strength up to 5.3% drift (top displacement=180 mm). Unlike other specimens, no fracture occurred in the boundary frame members. Ultimately, the load-carrying capacity of FSPW2 was decreased by the severe tearing of the infill plates. The tearing of the infill plates occurred at their centers where the two orthogonal tension fields repeatedly intersected each other under reversed cyclic loading.

In FSPW3, whose column shear capacity [$V_p = 0.6 f_{yw}(d_c - 2t_f)t_w$, f_{yw}=yield strength of the steel in the column web] was as low as 60% of the required shear strength ($V_u = 0.5 f_{py} t h_s \sin^2 2\alpha$), shear yielding was initiated in the first-story column at 2.7% drift (top displacement=90 mm) [see Fig. 7(a)]. At 3.6% drift (top displacement=120 mm), the stiffness and strength of FSPW3 significantly decreased. Fig. 6(b) shows its shear deformation that was concentrated in the first-story column.

In the CBF, at 0.9% drift (top displacement=30 mm), in-plane buckling occurred at the center of the compression braces on the first and second stories [Fig. 8(a)]. However, the beams, which were the same sizes as those used for FSPW2, were not designed to resist additional vertical load caused by buckling of the compression brace. Consequently, the second-story beam visibly deflected downward at 1.8% drift (top displacement=60 mm).

J. Struct. Eng. 2008.134:1495-1507.

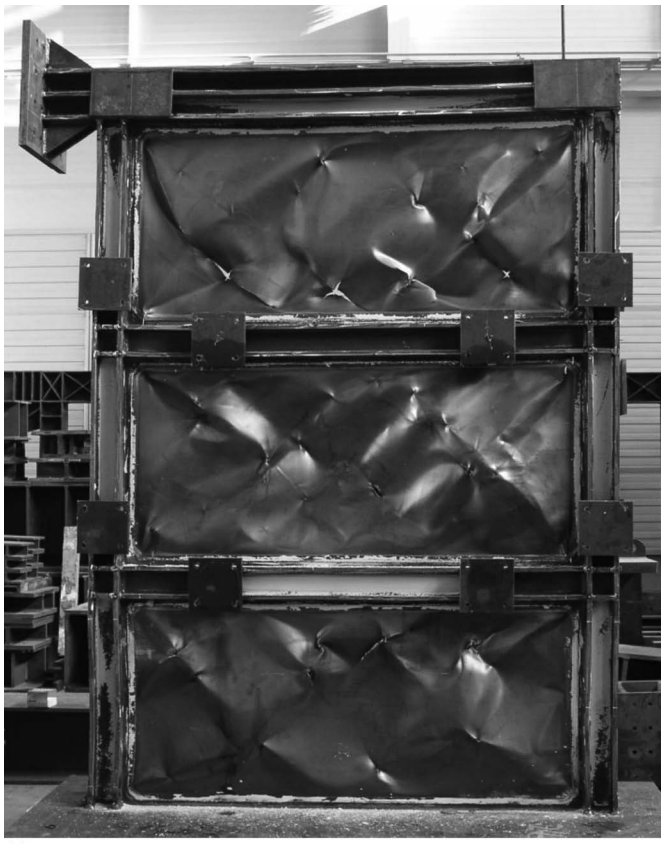

(a)

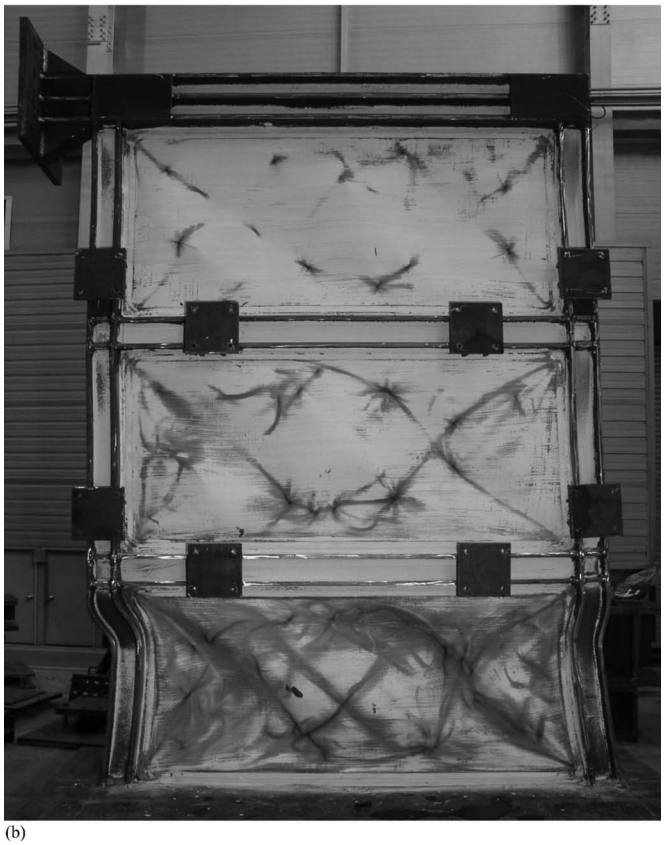

(b)

Fig. 6. Deformed shapes of FSPW specimens at the end of test: (a) FSPW2; (b) FSPW3

At the end of the test, the maximum deflections of the beams in the second and third stories were 19 and 16 mm, respectively. If the beams are designed according to the AISC Seismic Provisions (AISC 2005), the specimen CBF is expected to show better ductility.

In the MRF, plastic hinges were developed at the ends of beams and at the column base. At 5.3% drift (top displacement=180 mm), a fracture occurred at the tension flange of the third-story column that was connected to the top beam. At 7.1% drift (top displacement=240 mm), a fracture occurred at the beam-to-column joint in the second story.

Evaluation of Test Results

Deformation Capacity and Ductility

Table 5 summarizes the story drift and displacement ductility of the specimens tested in the present study and in previous studies. FSPW2, which was designed with a seismic compact column section, a ductile fish-plate detail, and flexible frame members (long span and small member sizes), showed the greatest deformation capacity (5.4% drift), which was close to that of the corresponding MRF specimen (6.3% drift). This result indicates that the deformation capacity of the shear-dominated steel plate wall designed with thin steel plates and ductile details can attain that of the MRF. However, from the viewpoint of earthquake design, the ductility capacity that represents the combined capacity of deformation and initial stiffness is more important than the deformation capacity. The displacement ductility of FSPW2 reached as much as 11.7, which was considerably greater than the value of 3.6 for the MRF, exhibiting low initial stiffness. The same trend was observed in the test of Caccese et al. (1993). The displacement ductility of the steel plate wall specimen M22 was 12.4, which was much greater than the value of 3.7 for the moment-resisting frame F0. It is noteworthy that both FSPW2 and M22 had very thin infill plates and seismic compact column sections with a very low width-thickness ratio. The test results show that the steel plate walls designed with such ductile details can have excellent ductility as well as high stiffness and strength. In the present study, the relationships between the ductility of the walls and the relevant design parameters were investigated in detail.

According to Park et al. (2007), the deformation and ductility capacities of steel plate walls are affected by their deformation mode. A steel plate wall exhibits either the moment frame action (shear-dominated behavior) or the cantilever action (flexure-dominated behavior), depending on the sizes of the boundary frame members and infill plates. The deformation mode of a steel plate wall can be evaluated by comparing its shear capacity (V_s) and flexural capacity (V_f). The calculations of V_s and V_f for the specimens tested in the present study are presented in the Appendix. The flexure-dominated wall ($V_f < V_s$) does not possess a large ductility capacity because excessive plastic deformation is required in the columns at the wall base [see Fig. 1(a)]. On the other hand, the shear-dominated wall ($V_s < V_f$) exhibits ductile behavior as yielding of the infill plates is distributed along the wall height [see Fig. 1(b)]. Fig. 9(a) and Table 5 show the relationships between the ratio of flexural capacity to shear capacity (V_f/V_s) and the roof displacement ductility (δ_{max}/δ_y) of the test specimens. The roof displacement ductility of the test specimens increases with V_f/V_s, and it ranges from 1.5 to 12.4. As shown in Fig. 9(a), several specimens, including SC2T (Park et al. 2007), SWT specimens (Elgaaly 1998), and S22 (Caccese et al. 1993), showed rela-

J. Struct. Eng. 2008.134:1495-1507.

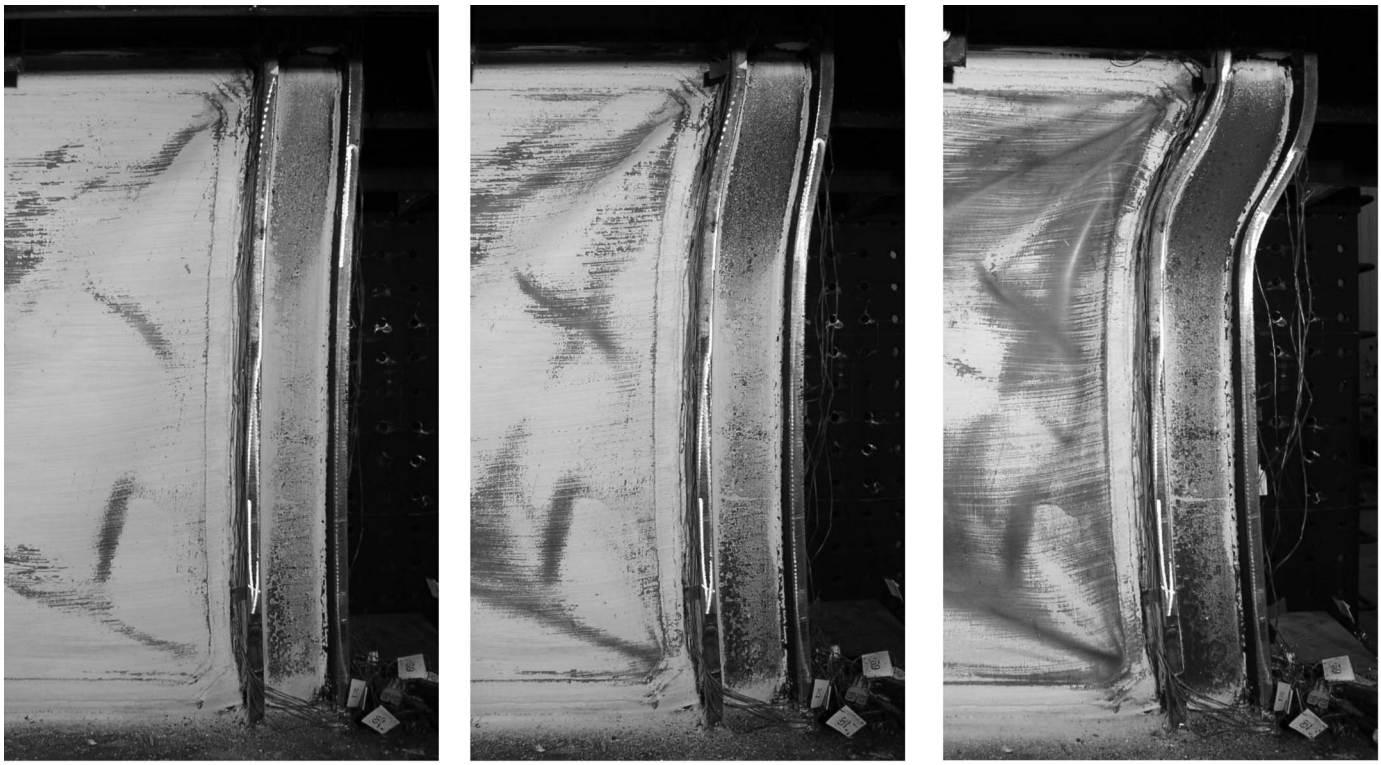

Fig. 7. Shear deformation at first-story column of FSPW3: (a) δ=90 mm; (b) δ=120 mm; and (c) δ=150 mm

tively low displacement ductility despite having high V_f/V_s ratios. The reason for the specimens exhibiting such low ductility will be discussed.

The actual displacement ductility of a wall is affected by the maximum interstory drift as well as the overall deformation mode of the wall. The maximum interstory drift in a specific story of a steel plate wall is determined by the local behavior of the frame members in that story. According to the existing test results, the most important local behavior affecting the interstory drift is the local buckling of columns. Fig. 9(b) and Table 5 show the relationship between the compactness ratio of the column flange (λ_{ps}/λ) and the maximum interstory drift ratio. $\lambda_{ps}=0.30\sqrt{E/f_{yf}}$ and f_{yf}=yield strength of the column flange steel. $\lambda=b_f/2t_f$. The maximum interstory drift ratio increases with the compactness ratio of the column flange. The interstory drift ratio of the test specimens ranges from 1.0 to 5.6%. As Elgaaly (1998) and Caccese et al. (1993) reported only the roof displacements in their studies, the average story drift calculated with the roof displacement was used as the interstory drift ratio of their specimens (see Table 5). The maximum interstory drift is expected to be greater than the average story drift.

The actual deformation capacity and ductility of a steel plate wall should be determined by considering both V_f/V_s in Fig. 9(a) and λ_{ps}/λ in Fig. 9(b). An example case is SWT15, which was tested by Elgaaly (1998). SWT15, with a low value of λ_{ps}/λ(=0.90), exhibited low ductility, although it had a high value of V_f/V_s [compare Figs. 9(a and b)]. Other SWT specimens, SC2T, and S22 are similar to SWT15. An opposite case is that of SPSW4, which was tested by Lubell et al. (2000). SPSW4, with a low value of V_f/V_s(=0.39), failed early due to instability initiated by the early yielding of the columns despite having a high value of λ_{ps}/λ [Compare Figs. 9(a and b)]. The cases of M14, M12, and S14 are similar. This result indicates that in order to maximize the deformation capacity and ductility of a steel plate wall, the requirements of both the deformation mode and the compactness of the column section should be satisfied. The overall displacement ductility of a steel plate wall should be evaluated such that the roof displacement ductility and the maximum story drift ratio do not exceed the values evaluated from Figs. 9(a and b), respectively. For multiple story walls that are subjected to different flexural moment and shear force at each story, V_f/V_s and λ_{ps}/λ should be evaluated in all the stories. The overall ductility of the multiple-story structure should be determined as the minimum of the potential ductility values that are evaluated by considering the V_f/V_s and λ_{ps}/λ in all the stories.

It should be noted that the results in Fig. 9 may overestimate the ductility and maximum interstory drift of actual full-size steel plate walls because the specimens in the tests were reduced-scale models. However, the structural capacity of the full-size steel plate walls can be indirectly evaluated by comparisons with the test results of the CBF and MRF, which are shown in Fig. 9.

Aspect Ratio of Infill Plate

The steel plate walls tested in the present study had a greater aspect ratio (l_p/h_p=2.2) as compared to those used in previous studies. Table 4 presents the stiffness and strength of the specimens. The ratios of the stiffness and strength of FSPW2 to those of FSPW1 with a low aspect ratio were 1.5 and 1.3, respectively. The stiffness and strength ratios were approximately the same as the ratio (=1.47) of the infill plate aspect ratio (l_p/h_p) of FSPW2 to that of FPSW1. This result indicates that the stiffness and shear strength of a wall increase proportionally with the depth of the infill plate (l_p, Fig. 2). As presented in Table 5, regardless of the

J. Struct. Eng. 2008.134:1495-1507.

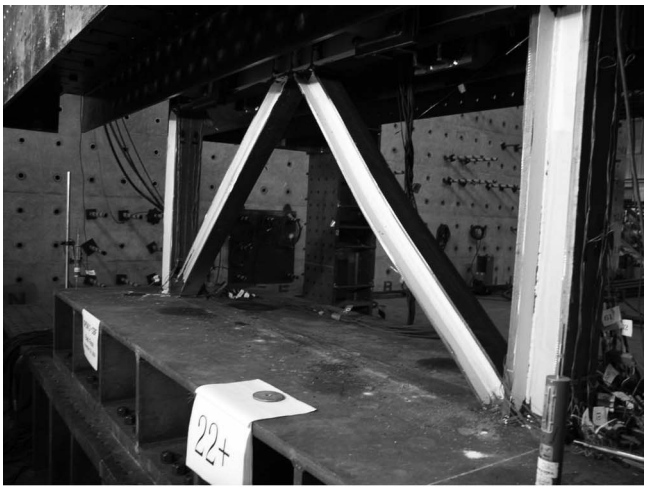

(a)

(b)

Fig. 8. Buckling of first-story brace in CBF: (a) $\delta=30$ mm; (b) $\delta=60$ mm

plate aspect ratio, the strengths of the test specimens were well predicted by the method proposed by Park et al. (2007) (see $V_{\text{pred}}/V_{\text{exp}}$). The predicted strength V_{pred} was determined to be the minimum between the shear capacity V_s and the flexural capacity V_f (see the Appendix).

Shear Capacity of Column

As mentioned, the columns in FSPW3 were designed to have 60% of the shear strength required for resisting the tension-field action of the infill plate. At 2.7% drift (top displacement =90 mm), inelastic shear deformation was initiated in the first-story columns in FSPW3. As shown in Figs. 6(b) and 7(c), the inelastic shear deformation was concentrated in the upper quarter of the column. Finally, a soft story developed on the first story of FSPW3. Table 5 presents the maximum interstory drifts of the specimens. In FSPW3, the maximum interstory drift on the first story was twice the drift on the upper stories. The large plastic deformation of the first story was maintained by the ductile behavior of the seismic compact column sections. However, if such a soft-story mechanism due to the shear yielding of columns occurs in a high-rise building, the overall deformation and ductility capacity of the building may significantly decrease because excessive plastic deformation is required for the columns on the soft story. The maximum interstory drift on the soft story cannot exceed the value shown in Fig. 9(b). Therefore, for the structural safety of multistory buildings, the columns should be designed to have sufficient shear strength for resisting the tension-field action of the infill steel plates.

Energy Dissipation Capacity of Shear-Dominated Wall

Fig. 10(a) shows the variations in the cumulative energy dissipation capacity of the specimens according to their story drifts. The energy dissipation capacity of FSPW2 was greater than the energy dissipation capacities of FSPW1 and FSPW3 with less deformation capacity. At 3.6% drift, the energy dissipation capacities on the first, second, and third stories of FSPW2 were in the ratio 1:1.09:0.80. This result indicates that the plastic deformation was uniformly distributed along the wall height. On the other hand, at the same drift, the energy dissipation capacities on the first, second, and third stories of FSPW3 were in the ratio 1:0.47:0.32. In FSPW3, the major part of the energy was dissipated on the first story where a large plastic deformation occurred due to the shear yielding of the columns. Before the buckling of the brace occurred at 0.9% drift ratio (top displacement=30 mm), the energy dissipation capacity of the CBF was similar to that of FSPW2. However, the total cumulative energy dissipation of FSPW2 was 5.8 times that of the CBF.

The energy dissipation capacity of the shear-dominated steel plate walls comprises the contributions by the infill plates and boundary frame. Thus, the energy dissipation of the infill plates can be evaluated by subtracting the energy dissipation of the moment frame action from the overall energy dissipation of the wall. Fig. 10(b) shows the energy dissipation per load cycle of FSPW2 (A) and the MRF (B). In FSPW2, at 2.7% drift (top displacement =90 mm), the ratio of the energy dissipation (per load cycle) of the boundary frame (B) to that of the infill plates (C=A−B) was 0.22. This result indicates that the major part of the energy was dissipated by the yielding of the infill plates. At the maximum drift, i.e., 5.3% drift (top displacement=180 mm), the ratio increased to 0.49, which indicates that the contribution of the moment frame action increased with the drift. However, at the maximum drift, the total cumulative energy dissipation of the infill plates was greater than three times that of the moment frame action [see Fig. 10(a)].

The energy dissipation of the infill plate (area=$l_p \times h_p$) can be calculated by using a simplified tension strip model, which is shown in Fig. 11(a). As the infill plate buckles on early loading, the strain energy developing in compression can be neglected [see Fig. 11(b)]. The strain ε_i in each tension strip is defined as

$$\varepsilon_i = \frac{\delta_s \cos\alpha}{h_p} = \frac{\delta_i \sin\alpha \cos\alpha}{h_p} \tag{1}$$

where δ_s=elongation of the tension strip; α=inclination angle of the tension strip [Eq. (14)]; and δ_i=lateral story drift on the ith story. The strain energy density u_s of each tension strip under a half load cycle is calculated as

$$u_s = (\varepsilon_i - \varepsilon_{\text{yi}}) f_{\text{py}} \tag{2}$$

where $\varepsilon_{\text{yi}}=f_{\text{py}}/E$; and E=elastic modulus of steel. The energy dissipation u_p of an infill plate under a full load cycle is calculated by multiplying $2u_s$ by the volume of the infill plate

J. Struct. Eng. 2008.134:1495-1507.

Table 5. Relationship between Deformation Mode and Ductility

Researcher	Specimens	V_{exp} (kN)	V_s (kN)	V_f (kN)	V_{pred} (kN)	V_{pred}/V_{exp}	V_f/V_s	Displ. ductility[a]	Compactness[b]	Story drift[c] (%)
Present study	FSPW1	1,388	1,304	1,520	1,304	0.94	1.16	8.1	2.11	4.5 (5.2[d])
	FSPW2	1,798	1,725	2,164	1,725	0.96	1.25	11.7	2.11	5.4 (5.6[d])
	FSPW3	1,531	1,702	1,726	1,702	1.11	1.01	8.6	1.90	3.6 (5.4[d])
	CBF	1,419	—	—	—	—	—	4.2	2.11	1.8 (2.5[d])
	MRF	453	—	—	—	—	—	3.6	2.11	6.3 (8.4[d])
Park et al. (2007)	SC2T[e]	1,663	1,520	2,366	1,520	0.91	1.56	6.4	1.18	3.4 (3.8[d])
	SC4T	2,480	2,333	2,366	2,333	0.94	1.01	4.4	1.18	2.6 (2.7[d])
	SC6T	3,020	2,943	2,366	2,366	0.78	0.80	3.8	1.18	2.6 (2.8[d])
	WC4T	1,520	2,221	1,644	1,644	1.08	0.74	3.8	0.61	1.7(2.3[d])
	WC6T	1,670	2,919	1,644	1,644	0.98	0.56	2.7	0.61	1.3 (1.4[d])
Behbahanifard (2003)	—	3,500	4,711	3,441	3,441	0.98	0.73	4.5	0.93	2.6 (3.4[d])
Lubell et al. (2000)	SPSW4	150	384	151	151	1.01	0.39	1.5	1.54	0.9 (1.0[d])
Elgaaly (1998)	SWT11[f]	370	435	567	435	1.17	1.30	3.6	0.65	2.1
	SWT12[e]	385	541	659	541	1.41	1.22	3.5	0.65	2.1
	SWT13[e]	343	541	652	541	1.58	1.20	3.4	0.65	1.8
	SWT14[f]	405	541	652	541	1.34	1.20	3.6	0.65	1.8
	SWT15	426	440	760	440	1.03	1.73	4.3	0.90	2.4
Driver et al. (1997)	—	3,080	4,845	2,571	2,571	0.83	0.53	4.7	0.93	2.1 (4.0[d])
Caccese et al. (1993)	M22[g]	178[h]	197	303	197	1.11	1.54	12.4[h]	1.45	5.4[h]
	M14	344	387	303	303	0.88	0.78	3.8	1.45	2.0
	M12	376	530	303	303	0.81	0.57	2.7	1.45	1.7
	S22[g]	142[h]	161	303	161	1.13	1.88	8.9[h]	1.45	3.9[h]
	S14	356	437	303	303	0.85	0.69	3.0	1.45	1.8
	F0[g](MRF)	72.9[h]	—	—	—	—	—	3.7[h]	1.45	5.7[h]

[a]Maximum roof displacement divided by yield roof displacement ($=\delta_{max}/\delta_y$).

[b]λ_{ps}/λ, λ=width-thickness ratio of column flange, and $\lambda_{ps}=0.30\sqrt{E/f_{yf}}$.

[c]Average story drift ($=\delta_{max}/h$).

[d]Maximum interstory drift.

[e]Failure at column base.

[f]Column buckling.

[g]Monotonic loading was applied after $\delta=50$ mm.

[h]Maximum values for monotonic loading.

$$u_p = 2\left(\frac{\delta_i \sin 2\alpha}{2h_p} - \frac{f_{py}}{E}\right) f_{py} t l_p h_p \tag{3}$$

The overall energy dissipation capacity of the three-story infill plates E_{DP} is calculated as

$$E_{DP} = \sum u_p = n_s u_p = 2n_s\left(\frac{\delta_i \sin 2\alpha}{2h_p} - \frac{f_{py}}{E}\right) f_{py} t l_p h_p \tag{4}$$

where n_s=number of stories with inelastic infill plates. For FSPW1 and FSPW2 in the present study, $n_s=3$ as all infill plates were uniformly yielded by the shear action.

The energy of the boundary frame is dissipated by the plastic hinges at the ends of the frame members. Assuming that the hysteretic behavior of the plastic hinges is elastoperfectly plastic, the energy of the boundary frame E_{HF} dissipating during a full load cycle can be calculated as

$$E_{HF} = 4\left(\sum M_{pi}\theta_{pi}\right) \tag{5}$$

where M_{pi}, θ_{pi}=plastic moment and rotation at a plastic hinge. In the steel plate walls tested in the present study, plastic hinges were developed at the bottom of the first-story columns, at the top of the third-story columns, and at the ends of the second- and third-floor beams [see Fig. 14(b)]. Therefore, assuming that all plastic hinges are subjected to the same rotation angle, E_{HF} is given by $4(\Sigma M_{pi}\theta_{pi})=4[2(M_{pc1}+M_{pb2}+M_{pb3}+M_{pc3})]\theta_p$. The plastic rotation ($\theta_p$) is approximately calculated as

$$\theta_p = (\theta_i - \theta_{yi}) = (\delta - \delta_e)/h \tag{6}$$

where θ_i and θ_{yi}=total rotation and yield rotation, respectively, at a plastic hinge; δ and δ_e=total lateral displacement and elastic lateral displacement of the boundary frame, respectively; and h=wall height. δ_e can be calculated by using an elastic frame model by assuming that the inflection points are located at the center of the beams and columns. For the single-span three-story walls tested in the present study

$$\delta_e = \sum \frac{V_{sf} h_s^2}{12E}\left(\frac{l}{I_{bi}} + \frac{h_s}{2I_{ci}}\right) \tag{7}$$

where l=center-to-center distance between the boundary columns; and I_{bi} and I_{ci}=moments of inertia of the boundary beam and column, respectively, on the ith story. As the flexural stiffness of the frame members softens early due to the Bauschinger effect, the energy dissipated by the boundary frame might be less than the elastoplastic energy E_{HF} in Eq. (5). However, during repeated cyclic loading, the flexural strengths of the beams and columns increase due to the cyclic strain-hardening effect of the steel;

J. Struct. Eng. 2008.134:1495-1507.

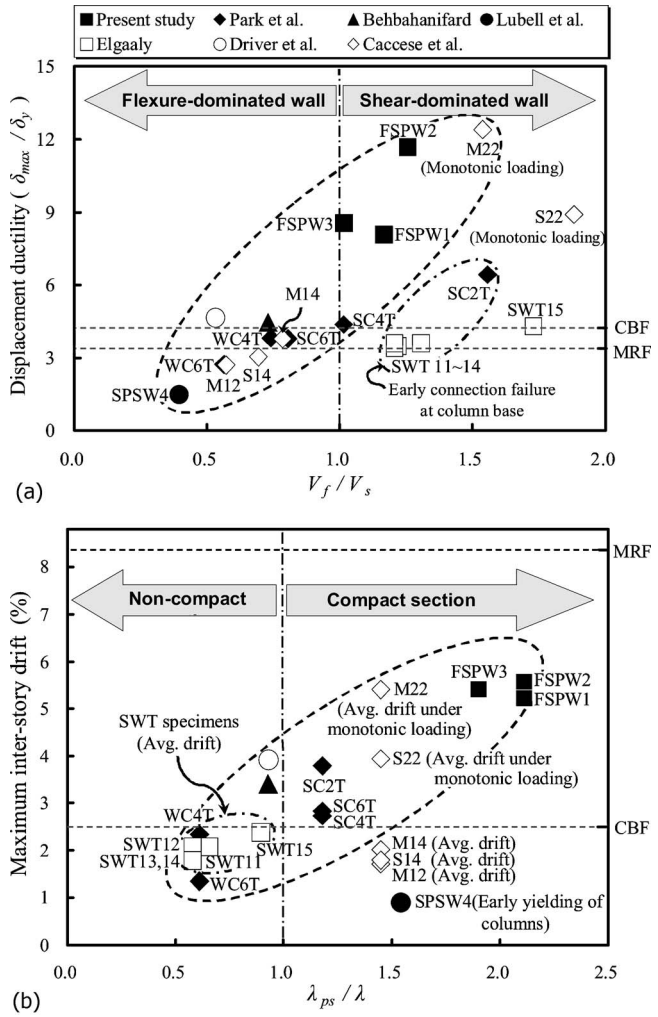

Fig. 9. Ductility and interstory drift capacities of steel plate walls: (a) Displacement ductility; (b) maximum interstory drift ratio

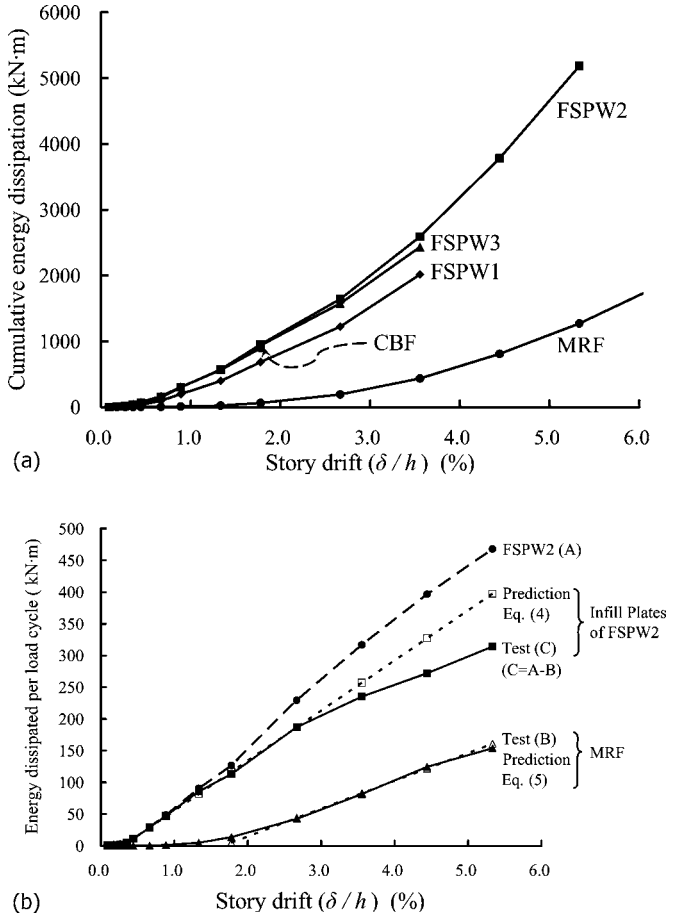

Fig. 10. Energy dissipation of test specimens: (a) Cumulative energy dissipation; (b) energy dissipation per load cycle (FSPW2, MRF)

consequently the energy dissipation increases. Thus, by considering the two opposite effects, the actual energy of the boundary frame E_{DF} was assumed to be the same as the elasto-perfectly plastic energy, i.e., $E_{DF}=E_{HF}$.

The predicted energy dissipation capacity (per load cycle) of FSPW2 is shown in Fig. 10(b). The proposed equations predicted the energy dissipation capacities of the infill plates and the boundary frame (MRF) with reasonable precision. However, after 2.7% drift (top displacement=90 mm), Eq. (4) overestimated the energy dissipation capacity of the infill plates. This is because as the lateral drift increased, a tearing fracture propagated at the center of the infill plates; consequently a portion of the displacement contributed by the plate tearing did not develop the plastic deformation of the infill plate.

The energy dissipation capacity (per load cycle) of a wall is defined as the sum of the contributions of the infill plates and the moment frame: $E_D=E_{DP}+E_{DF}$. The estimated energy dissipation capacity can be used to predict the cyclic behavior of steel plate walls. Fig. 12 shows the predicted load–displacement relationship of the shear-dominated steel plate walls FSPW1 and SC4T. The hysteretic load–displacement relationship was idealized by the symmetric bilinear curves defined using the initial stiffness and reloading stiffness. The initial stiffness of the wall was calculated by summing the stiffnesses of the infill plate and boundary frame: $K_i=K_{sp}+K_{sf}$. The initial stiffness of the infill plate is calculated as

$$K_{sp} = \beta \frac{V_{sp}}{\delta_{yp}} = \beta \frac{Etl \sin^2 2\alpha}{4 n_s h_s} \tag{8}$$

where δ_{yp}=yield displacement of the infill plate. δ_{yp} is calculated from the yield displacement of the idealized tension strip model in Fig. 11(a): $\delta_{yp}=(2n_s f_{py} h_s)/(E \sin 2\alpha)$. β(=0.7) is the stiffness modification factor that considers the initial imperfection of the infill plates (Park et al. 2007). The stiffness of the boundary frame can be calculated by using Eqs. (7) and (12): $K_{sf}=V_{sf}/\delta_e$. Based on the predicted initial stiffness K_i and the energy dissipation capacity E_D, the unloading or reloading stiffness of a wall can be

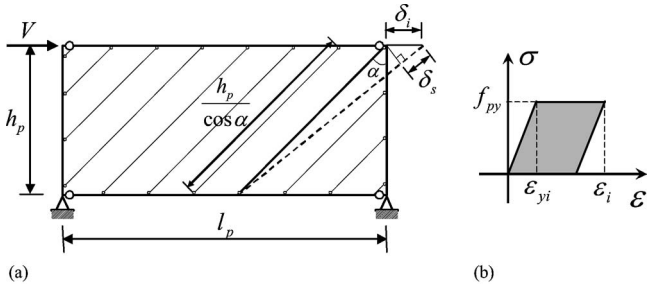

Fig. 11. Prediction of energy dissipation of infill plates: (a) Tension strip model; (b) idealized hysteretic behavior of a tension strip model

J. Struct. Eng. 2008.134:1495-1507.

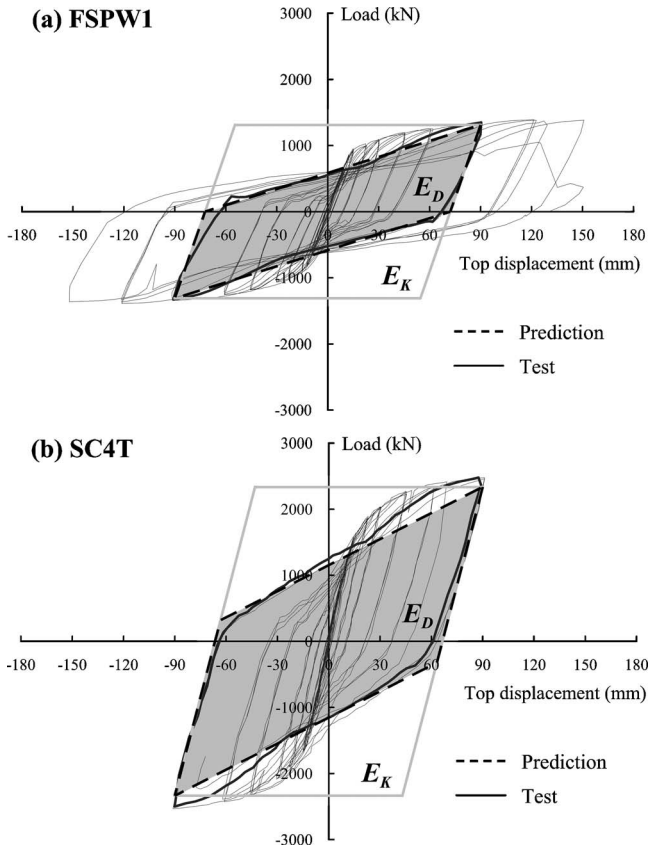

Fig. 12. Prediction of load–displacement relationship of shear-dominated steel plate walls

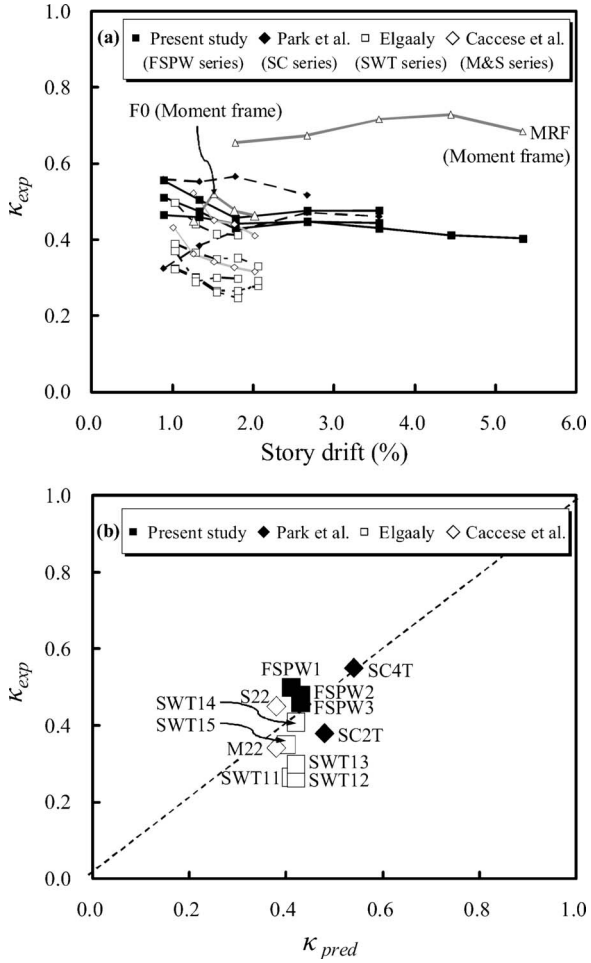

Fig. 13. Prediction of damping modification factors of shear-dominated steel plate walls

calculated so that the area enclosed by a cyclic curve is the same as the energy dissipation capacity (per load cycle) of the wall. For the specimens FSPW1 and SC4T,

$$K_r = \frac{(4V_s d_i - E_D)K_i - 4V_s^2}{4d_i^2 K_i - 4V_s d_i - E_D} \tag{9}$$

where d_i=top displacement of the specimens. As shown in Fig. 12, the proposed method predicted the cyclic behavior of the test specimens with reasonable precision.

By considering the energy dissipation capacity and initial stiffness, the damping modification factor (κ_{pred}) for a shear-dominated steel plate wall can be calculated. κ_{pred} is defined as the ratio of the predicted energy dissipation capacity E_D to the elastoplastic energy dissipation E_K: $\kappa_{pred}=E_D/E_K$, where $E_K=4V_s(d_i-V_s/K_i)$. Fig. 13(a) shows the variation of the damping modification factors κ_{exp} of the test specimens. The damping modification factors range from 0.25 to 0.57 for the steel plate wall specimens and from 0.45 to 0.73 for the MRFs. Fig. 13(b) compares the predicted damping modification factors κ_{pred} with the test results κ_{exp} at $d_i=3\delta_y$. The predictions agree well with the test results, except for the SWT specimens tested by Elgaaly (1998). The SWT specimens had bolt-connected infill plates and failed early due to a fracture at the column base. Thus, a portion of the total displacement caused by the bolt slip and the fracture of the column base did not contribute to the energy dissipation of the specimens. As a result, the proposed method overestimated the energy dissipation capacity of the SWT specimens. The damping modification factors κ_{exp} of the shear-dominated walls, excluding the SWT specimens, range from 0.32 to 0.57.

Conclusions

An experimental study was performed to investigate the potential maximum ductility and energy dissipation capacities of shear-dominated steel plate walls with thin infill plates. To maximize the ductility, the test specimens were designed with ductile details, including seismic compact column sections, full-penetration welded connection at the beam-to-column joints, and ductile fish-plate details. The findings obtained in the present study can be summarized as follows.

1. The respective values of displacement ductility and energy dissipation of the shear-dominated steel plate wall FSPW2 with thin infill plates were 2.8 times and 5.8 times those of the CBF, and 3.3 times and 2.8 times those of the MRF.
2. The shear-dominated steel plate wall designed with the ductile details exhibited an excellent deformation capacity that was close to that of the MRF.
3. The shear strength and energy dissipation capacity of the steel plate walls increased in proportion to the depth of the infill steel plate.
4. The overall displacement ductility of the steel plate walls increased with the ratio of the flexural capacity to the shear capacity. The maximum interstory drift ratio increased with the compactness of the column section.
5. The boundary columns must be designed to resist the shear force developed by the tension-field action of the infill plates.

J. Struct. Eng. 2008.134:1495-1507.

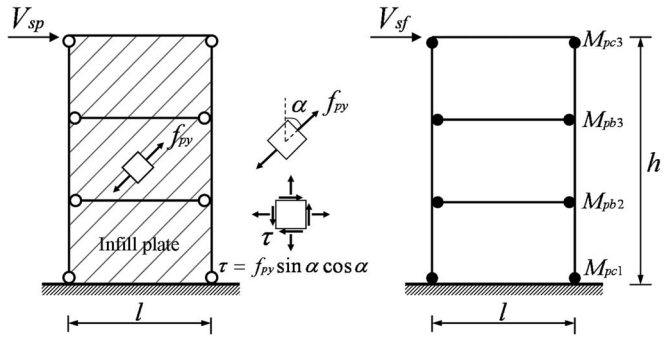

Fig. 14. Evaluation of shear strength (V_s): (a) tension-field action (V_{sp}); (b) moment frame action (V_{sf})

Otherwise, a soft story can be developed by the early shear yielding of the columns.

6. The energy dissipation capacity (per load cycle) of a steel plate wall can be estimated by using an idealized tension strip model. Based on the estimated energy dissipation capacity, the overall cyclic load–displacement relationship of the wall can be predicted.
7. The damping modification factors of the well-designed shear-dominated wall specimens range from 0.32 to 0.57, whereas that of the MRF specimens range from 0.45 to 0.73.

Acknowledgments

This research was financially supported by the Research Institute of Industrial Science and Technology (RIST) and Korea Institute of Construction and Transportation Technology Evaluation and Planning (KICTTEP) (Grant No. C105A1050001-05A0505-00210), and the writers are grateful to the authorities for their support.

Appendix

According to Park et al. (2007), the shear capacity V_s of a steel plate wall is defined as the sum of the contributions of the infill plate (V_{sp}) and the moment resisting frame (V_{sf}) (Fig. 14). For the single-span three-story walls tested in the present study

$$V_s = V_{sp} + V_{sf} \tag{10}$$

$$V_{sp} = \tau t l = f_{py} t l \sin\alpha \cos\alpha \tag{11}$$

$$V_{sf} = 2(M_{pc1} + M_{pb2} + M_{pb3} + M_{pc3})/h_{sh} \tag{12}$$

where τ=shear stress acting on the horizontal plane of the steel plate and h_{sh}=shear span of the specimen. For the specimens tested in the present study, the values of h_{sh} are identical to the wall height h. For other specimens, their plastic mechanisms and loading conditions were considered in the calculation of V_{sf}. Considering the slenderness effect, the flexural capacity V_f developed by the cantilever action is calculated as

$$V_f = A_c f_{cm} l/h_{sh} - P_g \delta/h_{sh} \tag{13}$$

where A_c=cross-sectional area of the boundary column; f_{cm}=allowable maximum stress of the boundary column ($f_{cm} \approx f_{cy} - P_g/A_c$); and P_g=gravity load applied on top of the specimen, if any. If the column does not have sufficient shear strength for resisting tension-field action, V_f is limited by the shear strength of the column.

In the Canadian Steel Design Standard (CSA 2001) and AISC Seismic Provisions (AISC 2005), the inclination angle of the tension-field action in the infill plate is specified as

$$\tan^4\alpha = \left(1 + \frac{tl}{2A_c}\right)\left[1 + th_s\left(\frac{1}{A_b} + \frac{h_s^3}{360I_c l}\right)\right]^{-1} \tag{14}$$

where A_b=cross-sectional area of the beam.

References

AISC. (2005). *Seismic provisions for structural steel buildings*, AISC, Chicago

Astaneh-Asl, A. (2001). "Seismic behavior and design of steel shear walls." *Steel TIPS Rep.*, Structural Steel Education Council, Moraga, Calif.

Behbahanifard, M. R. (2003). "Cyclic behavior of unstiffened steel plate shear walls." Ph.D. dissertation, Dept. of Civil Engineering, Univ of Alberta, Edmonton, Alberta, Canada.

Blogett, O. (1995). "Structural details to increase ductility of connections." *Steel TIPS Rep.*, Structural Steel Education Council, Moraga, Calif.

Caccese, V., Elgaaly, M., and Chen, R. (1993). "Experimental study of thin steel-plate shear walls under cyclic load." *J. Struct. Eng.*, 119(2), 573–587.

Canadian Standards Association (CSA). (2001). "Limit states design of steel structures." *CAN/CSA S16-01*, Willowdale, Ontario, Canada.

Driver, R. G., Kulak, G. L., Kennedy, D. J. L., and Elwi, A. E. (1997). "Seismic behavior of steel plate shear walls." *Structural Engineering Rep. No. 215*, Dept. of Civil Engineering, Univ of Alberta, Edmonton, Alberta, Canada.

Driver, R. G., Kulak, G. L., Kennedy, D. J. L., and Elwi, A. E. (1998). "Cyclic test of a four-storey steel plate shear wall." *J. Struct. Eng.*, 124(2), 111–120.

Elgaaly, M. (1998). "Thin steel plate shear walls behavior and analysis." *Thin-Walled Struct.*, 32, 151–180.

Hibbitt, Karlsson, and Sorenson Inc. (HKS). (2003). *ABAQUS standard*, version 6.4, Pawtucket, R.I.

Lubell, A. S., Prion, H. G. L., Ventura, C. E., and Rezai, M. (2000). "Unstiffened steel plate shear wall performance under cyclic loading." *J. Struct. Eng.*, 126(4), 453–460.

Park, H. G., Kwack, J. H., Jeon, S. W., Kim, W. K., and Choi, I. R. (2007). "Framed steel plate wall behavior under cyclic lateral loading." *J. Struct. Eng.*, 133(3), 378–388.

J. Struct. Eng. 2008.134:1495-1507.